

On the Extended Emission Around the Anomalous X-ray Pulsar 1E 1547.0–5408

S. A. Olausen¹, V. M. Kaspi¹, C.-Y. Ng¹, W. W. Zhu¹, R. Dib¹, F. P. Gavriil^{2,3}, and P. M. Woods^{4,5}

ABSTRACT

We present an analysis of the extended emission around the anomalous X-ray pulsar 1E 1547.0–5408 using four *XMM-Newton* observations taken with the source in varying states of outburst as well as in quiescence. We find that the extended emission flux is highly variable and strongly correlated with the flux of the magnetar. Based on this result, as well as on spectral and energetic considerations, we conclude that the extended emission is dominated by a dust-scattering halo and not a pulsar wind nebula (PWN), as has been previously argued. We obtain an upper limit on the 2–10 keV flux of a possible PWN of $4.7 \times 10^{-14} \text{ erg s}^{-1} \text{ cm}^{-2}$, three times less than the previously claimed value, implying an efficiency for conversion of spin-down energy into nebular luminosity of $<9 \times 10^{-4}$ (assuming a distance of 4 kpc). We do, however, find strong evidence for X-ray emission from the supernova remnant shell surrounding the pulsar, as previously reported.

Subject headings: pulsars: individual (1E 1547.0–5408) — stars: neutron — X-rays: stars

1. Introduction

Anomalous X-ray pulsars (AXPs) and soft gamma repeaters (SGRs) are generally accepted as belonging to the class of neutron stars known as ‘magnetars.’ These sources are characterized by long (2–12 s) spin periods and spin-down rates that imply extremely high surface dipole magnetic fields of 10^{14} – 10^{15} G (see Woods & Thompson 2006 and Mereghetti 2008 for reviews). It is thought that their large X-ray luminosities are powered by the decay of these powerful magnetic fields, and

¹Department of Physics, Rutherford Physics Building, McGill University, 3600 University Street, Montreal, Quebec H3A 2T8, Canada

²NASA Goddard Space Flight Center, Astrophysics Science Division, Code 662, Greenbelt, MD 20771, USA

³Center for Research and Exploration in Space Science and Technology, University of Maryland Baltimore County, 1000 Hilltop Circle, Baltimore, MD 21250, USA

⁴Dynetics, Inc., 1000 Explorer Boulevard, Huntsville, AL 35806, USA

⁵Corvid Technologies, 689 Discovery Drive, Huntsville, AL 35806, USA

fracturing of the crust and reconfiguration of the magnetic field lines produce the glitches, bursts, and X-ray variability seen in these sources (Thompson & Duncan 1995, 1996; Thompson et al. 2002).

One important open question regarding AXPs and SGRs is whether they produce particle outflows akin to those seen in conventional rotation-powered pulsars. The latter are well known to produce often spectacular ‘pulsar wind nebulae’ (PWNe), the classic example of which is the Crab Nebula (see, e.g., Kaspi et al. 2006; Gaensler & Slane 2006; Kargaltsev & Pavlov 2008, for reviews). Such nebulae, evident particularly at radio and X-ray energies, are the result of synchrotron emission due to pulsar-produced relativistic electrons and positrons, as they spiral in the ambient magnetic field. Given the large magnetic energy reservoir hypothesized to exist in AXPs and SGRs, particle outflows seem reasonable to consider, and indeed have been suggested to be present ubiquitously in magnetars, either in continuous or sporadic forms (Thompson & Blaes 1998; Harding et al. 1999). This idea was initially buoyed by the claim of an apparent wind nebula associated with SGR 1806–20 (Murakami et al. 1994). Although the latter association was later disproved (Hurley et al. 1999), the possibility of a nebula-producing magnetar wind has not been. Extended radio emission was unambiguously identified following one SGR giant flare (Gaensler et al. 2005; Taylor et al. 2005; Gelfand et al. 2005; Fender et al. 2006), but is thought to be from relativistic, weakly baryon-loaded magnetic clouds (Lyutikov 2006) or from a baryonic outflow (Gelfand et al. 2005; Gelfand 2007), and associated exclusively with the flare. Recently Rea et al. (2009) have suggested that an unusual X-ray nebula surrounding the relatively high- B Rotating Radio Transient (RRAT) J1819–1458 is magnetically powered, though the mechanism for this is unclear.

The X-ray source 1E 1547.0–5408 was discovered with the *Einstein* X-ray satellite in 1980 by Lamb & Markert (1981), but only recently was it suggested to be a magnetar candidate on the basis of its spectrum, variable nature, and likely association with the supernova remnant (SNR) shell G327.24–0.13 (Gelfand & Gaensler 2007). Radio observations of the source by Camilo et al. (2007) revealed pulsations at a period of 2.1 s and the measured spin-down rate implied a surface magnetic field strength of 2.2×10^{14} G and a spin-down luminosity of $\dot{E} = 1.0 \times 10^{35}$ erg s $^{-1}$. 1E 1547.0–5408 is thus the fastest-rotating and highest- \dot{E} magnetar yet known.¹ Although observations in 2006 showed the source to be in quiescence, a 2007 *XMM-Newton* observation showed it to be in a high, apparently post-outburst state (Halpern et al. 2008). In 2008 October and again on 2009 January 29, 1E 1547.0–5408 underwent strong outburst events, experiencing dramatic increases in its X-ray luminosity and exhibiting many SGR-like bursts within a few hours. For further details on these outbursts and the source’s history, see Israel et al. (2010), Kaneko et al. (2010), Ng et al. (2011), Bernardini et al. (2011), Scholz & Kaspi (2011), and Dib et al. (2011).

In observations of 1E 1547.0–5408 taken with *Swift* and *XMM-Newton* following the 2009 outburst, Tiengo et al. (2010) observed dust-scattering X-ray rings centered on the magnetar and derived from them a source distance of ~ 4 –5 kpc. They also found evidence of time variable diffuse

¹See the McGill SGR/AXP Online Catalog at <http://www.physics.mcgill.ca/~pulsar/magnetar/main.html>.

emission around the source which they attributed to dust scattering of the bursts and of the persistent X-ray emission.

Meanwhile, Vink & Bamba (2009, hereafter VB09), analyzing *Chandra* and *XMM-Newton* observations of the source taken in 2006 when it was in quiescence, detected extended emission and characterized it as the result of a PWN, in analogy with those seen around rotation-powered pulsars. They argued for a PWN based on the high flux level of the extended emission, and because it appeared to have a harder spectrum than the point source. This would make 1E 1547.0–5408 unusual among the known magnetars, as no other such source has been shown to power such emission. They also showed the presence of extended X-ray emission coincident with the SNR shell.

Here we present an analysis of the extended emission around 1E 1547.0–5408 using multi-epoch *XMM* data, in which the source flux varies strongly, as does the putative nebular emission. We show conclusively that the putative PWN reported by VB09 is in fact dominated by dust scattering, rather than by emission from any pulsar outflow.

2. Observations

We obtained an observation of 1E 1547.0–5408 with the *XMM-Newton Observatory* on 2010 February 10 in order to track the star’s properties as it decayed to quiescence after the 2009 outburst. We also reanalyzed three archival *XMM-Newton* observations of the source: one in 2006 with the source in quiescence, the 2007 post-outburst observation, and one taken 2 weeks after the 2009 outburst. For each observation, the data from the two EPIC MOS cameras (Turner et al. 2001) were not suitable for our analysis, either because the operating mode provided too small a field of view or because the data were highly piled-up. We therefore restricted our analysis to data from the EPIC pn camera (Strüder et al. 2001), which had no such issues. The data from all four observations were analyzed using the *XMM-Newton* Science Analysis System (SAS) version 10.0.2² with calibrations updated 2010 July 29. Each observation was filtered for times of strong background flaring that sometimes occur in *XMM-Newton* data, and two bursts were removed from the 2009 data. Details of each of the four observations, including the total pn exposure time after removing the bad time intervals, are listed in Table 1.

3. Imaging Analysis and Results

In order to search for and characterize any extended emission around 1E 1547.0–5408, we began by removing all point sources detected in the field of each observation other than the magnetar,

²See <http://xmm.esac.esa.int/sas/10.0.0/>

as well as the out-of-time pn events present in the 2009 observation. To construct a radial profile, we extracted events from concentric annuli having width $2''$ centered on the position of the star, as determined by a standard centroid search algorithm. The number of counts in each bin was divided by both the geometric area of each extraction region and the mean exposure time therein as determined from the unvignetted exposure map. This procedure corrects for the chip gaps, dead pixels, and removed regions on the detector.

The radial profile of a point source in *XMM-Newton* is given by the energy-dependent, radially averaged point-spread function (PSF). Using the SAS task `eradial` we extracted from instrument calibration files the theoretical PSF at 1 keV energy intervals from 1 to 12 keV for each observation. These component PSFs were weighted such that the PSF at energy E_i was given the weight $W(E_i) = \frac{N_{10}(|E-E_i| < 0.5 \text{ keV})}{N_{10}(E)}$, where $N_{10}(E)$ is the total number of counts within $10''$ of the source position. They were then summed to produce a weighted PSF, $S(r)$. Finally, by scaling $S(r)$ using the formula

$$P(r) = a \cdot S(r) + b,$$

we created an expected point-source radial profile $P(r)$ for each observation. Here, b is a spatially uniform background count rate found by averaging the count rate in all the bins of the observed profile a sufficient distance away from the source. The normalization factor a was derived via a least-squares fit of $P(r)$ to the first five bins ($10''$) of the observed radial profile, under the assumption that the contribution of any extended emission to the profile in that region would be minimal. We found, however, that the least-squares fit tended to be poor, especially for the observations with higher count rate and thus better statistics. This suggested that the uncertainty on a based on the χ^2 was not reliable because of additional systematic errors affecting the fit. For example, in addition to possible contamination by extended emission, the $2''$ size chosen for the radial bins oversamples the $4'' \times 4''$ square pixels of the pn detector. Therefore, in order to better estimate the uncertainty, we obtained a range of possible values for a by making a least-squares fit of $P(r)$ to any four of the first five and any five of the first six bins of the observed profile. Our uncertainty estimate was then given by $\delta a = (a_{\text{max}} - a_{\text{min}})/2$.

The 2010 radial profiles of 1E 1547.0–5408 in the 1–6 keV and 6–12 keV energy bands are shown in Figure 1. Below 6 keV the observed profile has a significant excess of counts over the expected point-source profile, extending out to $r \approx 4.5''$; conversely, above 6 keV no excess is detected and the observed profile is consistent with a point source. Radial profiles constructed from the three archival data sets display similar results, although the shape and extent of the excess vary among the observations, and the three dust-scattering rings reported in Tiengo et al. (2010) are visible in the 2009 data. We therefore confirm the presence of extended emission around 1E 1547.0–5408 below 6 keV as previously reported by VB09 and Tiengo et al. (2010). We also find that the extended emission is brighter at low energies (< 3 keV), in line with the soft spectrum reported by VB09.

In Figure 2, we plot the 1–6 keV count rate of the extended emission, I_{ext} , as a function of the total background-subtracted point-source count rate, I_{ps} , for two regions: region A, an annulus centered on the source with radius $20'' < r < 40''$; and region B, a similar annulus but with radius

$40'' < r < 150''$. In both regions we find a tight correlation between the two quantities; in fact, the first three points (2006, 2007, and 2010) fit well to a straight line, although the fourth point (2009) lies above the extrapolated linear fit in both regions A and B (but see Section 4.2). The extended emission flux varies wildly between observations, increasing and decreasing along with the flux of the pulsar. For example, in region A the extended emission brightened by a factor of nearly 50 between the 2006 and 2009 observations, and by the following year it had faded by almost a factor of three.

Figure 3 shows the fractional intensity of the extended emission, $I_{\text{frac}} = I_{\text{ext}}/I_{\text{ps}}$ in regions A and B for all four observations of 1E 1547.0–5408. The most prominent feature in both regions is that I_{frac} in 2006 is notably higher than in the other three observations, particularly in region B.

3.1. Spectral Analysis

Because of contamination from the broad wings of the *XMM-Newton* PSF, we could not simply extract spectra of the extended emission from regions A and B. For example, in each observation, less than half of the total background-subtracted counts found in region A were contributed by the extended source. Therefore, we instead computed a simple hardness ratio for the extended emission, $\text{HR}_{\text{ext}} \equiv I_{\text{ext}}(3\text{--}6 \text{ keV})/I_{\text{ext}}(1\text{--}3 \text{ keV})$, and we list in Table 2, for all four observations, these hardness ratios in regions A and B. For comparison, the table also lists the hardness ratio of the point source, $\text{HR}_{\text{ps}} \equiv I_{\text{tot}}(3\text{--}6 \text{ keV})/I_{\text{tot}}(1\text{--}3 \text{ keV})$, where I_{tot} is the background-subtracted count rate within $10''$ of the source position.

We find that in region A, $\text{HR}_{\text{ext}} < \text{HR}_{\text{ps}}$ for all four observations, meaning that the extended emission has a softer spectrum than the point source, although in 2006 the hardness ratio is smaller by only 1.5σ . In region B, the results are the same as above for all but the 2006 observation, where the extended emission spectrum is instead harder than the source spectrum. This behavior is further illustrated in Figure 4, which shows the 2006 hardness ratio of the extended emission as a function of distance from the source, beginning at $20''$ (the first bin provides the hardness ratio of the point source itself).

Finally, assuming an absorbed power-law spectrum, the hardness ratios in Table 2 can be used to constrain the photon index Γ and the flux of the extended emission. For example, taking $N_{\text{H}} = 2.75 \times 10^{22} \text{ cm}^{-2}$ as in VB09, we find that the 2–10 keV unabsorbed flux of the extended emission in region A varied from a minimum of $\sim 4 \times 10^{-14} \text{ erg s}^{-1} \text{ cm}^{-2}$ (for $\Gamma \approx 4$) in 2006 to a maximum of $\sim 3 \times 10^{-12} \text{ erg s}^{-1} \text{ cm}^{-2}$ (for $\Gamma \approx 3$) in 2009.

4. Discussion

Our analysis has confirmed the presence of extended emission around 1E 1547.0–5408, visible in four observations taken at very different stages of its flux history. VB09 previously detected extended emission around this source based primarily on a 2006 *Chandra* observation and interpreted it as a PWN and, farther out, the X-ray counterpart of SNR G327.24–0.13. Here we reexamine this interpretation in light of our new data.

4.1. A Pulsar Wind Nebula?

In the context of conventional rotation-powered pulsars, given the low spin-down power of 1E 1547.0–5408, we generally would not expect it to harbor a bright PWN in X-rays. For $\dot{E} = 10^{35} \text{ erg s}^{-1}$, the typical X-ray efficiency of a PWN is about 10^{-4} (Kargaltsev & Pavlov 2008). Even allowing for the X-ray efficiency to be up to an order of magnitude greater, this predicts an unabsorbed PWN flux of $\lesssim 5 \times 10^{-14} (d/4 \text{ kpc})^{-2} \text{ erg s}^{-1} \text{ cm}^{-2}$ in the 0.5–8 keV range for 1E 1547.0–5408. On the other hand, the putative PWN as suggested by VB09 has an unabsorbed flux of $\sim 1 \times 10^{-12} \text{ erg s}^{-1} \text{ cm}^{-2}$ in the same band. Thus, if the extended emission is entirely rotation-powered, this would require an unusually high X-ray efficiency of over 1%. This problem could be alleviated, however, by hypothesizing that magnetic power could be contributing to the nebula, as has been suggested by Rea et al. (2009) for RRAT 1819–1458.

However, another issue is the soft spectrum of the putative PWN. The hardness ratios in Section 3.1 suggest a power-law spectrum with photon index $\Gamma \approx 3\text{--}4$, a range that is consistent with the value reported in VB09 ($\Gamma = 3.4 \pm 0.4$). This is much softer than previously reported PWNe, which typically have $\Gamma \approx 1.5\text{--}2$ (Kargaltsev & Pavlov 2008), although VB09 proposed that the discrepancy could be explained as being somehow a result of the magnetar nature of 1E 1547.0–5408.

A more pressing problem with the PWN interpretation is its failure to explain the strong flux correlation seen in Figure 2. First, PWNe in rotation-powered pulsars have not been seen to have large luminosity variations as are observed for 1E 1547.0–5408. Even if energy injection due to outbursts played a role, we show here that the observed fading time is incompatible with a synchrotron origin. First, to estimate the magnetic field strength in the putative PWN, we consider as an analogy the 2004 flare of SGR 1806–20, which was accompanied by nebular radio emission. In that event, a total energy of $2 \times 10^{46} \text{ erg}$ was released (Palmer et al. 2005). Lyutikov (2006) proposed that the event could produce relativistic, weakly baryon-loaded magnetic clouds analogous to a solar coronal mass ejection, and deduced a total energy of $8 \times 10^{44} \text{ erg}$ for the relativistic electrons plus magnetic field, with an average magnetic field B of 0.1 G within a radius $\sim 1.5 \times 10^{16} \text{ cm}$. As the nebula expands, the field strength decays with the volume V as $V^{-1/2}$ or $V^{-2/3}$, depending on whether the field is tangled (Gaensler et al. 2005). Assuming the former case, we have scaled these values to those appropriate for the properties of 1E 1547.0–5408 and

find a conservative B -field estimate of $<80 \mu\text{G}$ at $30''$, which corresponds to 1.8×10^{18} cm from the source. We note that the B -field is much lower for the latter field decay case. The synchrotron cooling timescale is then $\tau_{\text{syn}} = 37(B/1 \mu\text{G})^{-3/2}(\varepsilon_\gamma/1 \text{ keV})^{1/2} \text{ kyr} \gtrsim 120 \text{ yr}$ for particles emitting at $\varepsilon_\gamma=6 \text{ keV}$. This is incompatible with the flux decay timescale observed and shown in Figure 2, in particular between 2009 and 2010.

The above theory suggests that the particle energy was about 4% of the burst fluence for SGR 1806–20. The total burst fluence for the 2009 event of 1E 1547.0–5408 was measured to be $\gtrsim 5 \times 10^{43} (d/10 \text{ kpc})^2 \text{ erg}$ by Mereghetti et al. (2009), and estimated to be in the range 10^{44} – 10^{45} erg by Tiengo et al. (2010). Taking the uppermost value of 10^{45} erg would give an injected particle energy of 4×10^{43} erg. Assuming this results in synchrotron emission from the radio regime up to 6 keV, with a typical photon index of 1.5, we find a power of $1.1 \times 10^{32} \text{ erg s}^{-1}$, corresponding to a flux of $6 \times 10^{-14} (d/4 \text{ kpc})^{-2} \text{ erg s}^{-1} \text{ cm}^{-2}$ between 1 and 6 keV. This is well below the observed extended emission flux in 2009.

For completeness, we note that there are alternative models proposing baryonic outflows for the magnetar outbursts (Gelfand et al. 2005; Granot et al. 2006). If this is the case, then no detectable synchrotron X-rays are expected.

4.2. Dust-scattering Halo

Extended emission around an X-ray source can be produced by the scattering of X-rays off dust particles between the source and observer. The flux of such a dust-scattering halo is expected to be proportional to the source flux (Mathis & Lee 1991). Returning to Figure 2, then, for a dust-scattering halo, all of the points should fit well to a straight line (allowing for some scatter because the source spectrum did not remain constant). This is indeed the case for the first three points, although the 2009 point lies above the linear fit. In order to fit with the linear trend, the 2009 source flux would have to be 15%–20% higher than what we observed. However, because the scattered photons in a dust halo travel a longer path than photons observed directly from the source, the halo flux depends in a complicated manner on the recent history of the source flux over a period of hours or days (Mauche & Gorenstein 1986). The 2009 *XMM* observation of 1E 1547.0–5408 was taken only 13 days after its January outburst, at which time the magnetar’s flux was decaying following a power law of index $\alpha = -0.34$ to -3.1 (Bernardini et al. 2011; Scholz & Kaspi 2011). As a result, the source would have been bright enough to produce the observed halo 4.5–5.5 days prior to the observation, not an unreasonable timescale for the evolution of a dust halo. We therefore conclude that the observed variability in the extended emission flux is entirely consistent with a dust-scattering halo.

VB09 rejected the dust-scattering halo interpretation of the extended emission based on two arguments. The first one is that the extended emission around 1E 1547.0–5408 had a harder spectrum than the source itself. A dust halo, on the other hand, is expected to have a softer

spectrum than the source because the scattering cross section has an inverse-square dependence on energy. From the hardness ratios in Table 2 we find that, contrary to the claim by VB09, the extended source in region A has an unambiguously softer spectrum than the magnetar in 2007, 2009, and 2010, supporting the interpretation of dust scattering. In 2006, the hardness ratios suggest a softer spectrum too, although the difference is not statistically significant. For comparison, though, VB09 reported that the photon index Γ of the ‘PWN’ differed from that of the point source by only 1σ , which is not statistically significant either. We cannot, therefore, conclude that the spectrum of the extended emission in region A supports either interpretation in 2006. It should be noted, however, that be it harder or softer than the point source, the extended emission in 2006 still has a much softer spectrum than any previously reported PWN, as discussed above.

Table 2 also indicates similar results for region B as in region A. The extended emission shows a softer spectrum than the magnetar in all observations except 2006. Again, we note that although the extended emission spectrum is harder than the point source in 2006, it is still very soft overall.

Our investigations so far strongly support that the extended emission observed around 1E 1547.0–5408 in regions A and B is dominated by a dust-scattering halo, at least in 2007, 2009, and 2010, although this interpretation is less clear in 2006. We now examine the other argument given in VB09 against dust scattering: that the extended emission was too bright, especially above 3 keV, to be a dust halo. They estimated the expected fractional halo intensity and the dust-scattering optical depth τ_{sca} based on models by Predehl & Schmitt (1995) and Draine (2003), which depend on the absorption column N_{H} , the X-ray energy E , and a parameter β describing the distribution of the dust between source and observer. Following a similar procedure, we assumed an effective energy $E = 2$ keV for the 1–6 keV photons based on the spectrum of the magnetar, took $\beta = 1$ (meaning most of the dust is close to the source) and $\tau_{\text{sca}} = 1.5$, as in VB09, and calculated I_{frac} for regions A and B. This gives $I_{\text{frac}} = 0.08$ for region A and $I_{\text{frac}} = 0.18$ for region B, which are in a good agreement³ with the 2010 values in Figure 3, suggesting that dust scattering is adequate to explain the brightness of the extended emission, at least in 2010. For pure dust scattering we expect I_{frac} in each region to be the same for each observation, except in 2009 where it should be higher due to source variability as discussed above. Indeed, there is a good agreement between the 2007, 2009, and 2010 observations, but the 2006 value of I_{frac} stands out. In region A, it is 3σ higher than what is expected from the 2007 and 2010 data, and in region B an even larger increase is evident, with I_{frac} being $>10\sigma$ higher in 2006 than in any subsequent observation.

The best explanation for all of our results is that the extended emission around 1E 1547.0–5408 consists of a dust-scattering halo plus an additional component independent of the source flux. This secondary component is significant mainly in region B and becomes noticeable only when the halo is faint, as is the case for the 2006 observation. In order to better quantify it we return to Figure 2. For pure dust scattering, the linear fits in the diagram should pass through the origin. As seen

³In region B, the calculated I_{frac} is actually below the observed value by 3σ . However, if we subtract the non-dust contribution to the extended emission from the SNR (see below and Table 3) then the two values are in full agreement.

from the inset, however, both fits have a positive y -intercept, suggesting that some of the extended emission does not come from the dust halo. In Table 3, we list the values of the y -intercepts for regions A and B and the extended emission count rate in 2006, and we calculate the fraction of the latter that was not contributed by dust scattering.

We find that in region B, $75\% \pm 6\%$ of the extended emission in 2006 is not from the dust halo. Since our region B mostly corresponds to the SNR region ($45'' < r < 174''$) from VB09 and therefore to the location of the radio SNR shell, we conclude that the X-ray counterpart of this shell is the source of the non-dust extended emission here.

Region A corresponds roughly to the ‘PWN’ region ($4'' < r < 45''$) from VB09, noting that the broad PSF of *XMM-Newton* restricts us to $r > 20''$. Unlike farther out, the 2006 extended emission in region A is still dominated by the dust halo; only $36\% \pm 12\%$ of it comes from another source. In fact, since the significance is only 3σ above zero, it is possible that dust scattering alone is sufficient to explain all of the extended emission in region A. Nevertheless, we can use the parameters in Table 3 to estimate an upper limit on the flux of a possible PWN, assuming an absorbed power-law spectrum with $N_{\text{H}} = 2.75 \times 10^{22} \text{ cm}^{-2}$, as in VB09, and a photon index of $\Gamma = 2$, as is typical of PWNe. We find a 3σ upper limit⁴ on the 2–10 keV unabsorbed flux of $\lesssim 4.7 \times 10^{-14} \text{ erg s}^{-1} \text{ cm}^{-2}$, corresponding to a luminosity of $9 \times 10^{31} (d/4 \text{ kpc})^2 \text{ erg s}^{-1}$. This implies an X-ray efficiency of $L_{\text{X}}/\dot{E} \lesssim 9 \times 10^{-4} (d/4 \text{ kpc})^2$. We also repeated our estimation for a softer PWN spectrum of $\Gamma = 3$, but found that the 2–10 keV upper limit was largely insensitive to changes in Γ .

5. Conclusions

In this paper, we have examined multi-epoch *XMM-Newton* data for the magnetar candidate 1E 1547.0–5408 and we show that the observed extended emission surrounding the source is dominated by dust-scattered magnetar emission. Specifically we find that the luminosity of the nebular emission is proportional to the source flux, as expected for dust scattering, but not seen in any known PWN or other magnetar candidate. Additional strong evidence for dust-scattering comes from spectral and energetics arguments, as well as from the disagreement between the observed nebular variability time scale and the expected synchrotron loss time in the PWN interpretation. We note that contrary to a previous claim (VB09), even in 2006 when the source was relatively faint, $64\% \pm 12\%$ of the nebular emission is from dust scattering. We cannot, however, rule out the presence of a faint PWN with luminosity $\lesssim 9 \times 10^{31} (d/4 \text{ kpc})^2 \text{ erg s}^{-1}$ in the 2–10 keV band, a limit three times lower than the previously claimed detection ($\sim 2.9 \times 10^{32} \text{ erg s}^{-1}$ from VB09). Deep observations of this source when the magnetar is in quiescence are necessary to test this hypothesis. We do, on the other hand, find strong evidence for non-dust-scattered extended X-ray

⁴In this case, the most stringent upper limit found was based on the non-detection of extended emission above 6 keV, not the parameters from Table 3.

emission at angular distance $\sim 40''$ – $150''$, which we argue is from the SNR shell surrounding the pulsar, as previously reported by VB09.

With the absence of evidence for a PWN surrounding any AXP or SGR, now including 1E 1547.0–5408, previous models for the production of PWNe by magnetars (Thompson & Blaes 1998; Harding et al. 1999) remain unsupported. On the other hand with clear evidence for the existence of PWNe surrounding many high-magnetic-field radio pulsars (e.g., PSR J1846–0258: Helfand et al. 2003; PSR J1119–6127: Gonzalez & Safi-Harb 2003) which generally have substantially higher spin-down luminosities than any known AXP or SGR, the production of the relativistic particle wind necessary to generate an observable PWN seems intimately tied to the rotation-derived power, rather than that from magnetic-field decay. This then makes the detection of the surprisingly bright X-ray PWN surrounding the presumably rotation-powered but relatively high- B RRAT PSR J1819–1458 (Rea et al. 2009) particularly interesting and worthy of follow-up.

This research is based on observations obtained with *XMM-Newton*, an ESA science mission with instruments and contributions directly funded by ESA Member States and NASA. V.M.K. receives support from NSERC via a Discovery Grant, FQRNT via the Centre de Recherche Astrophysique du Québec, CIFAR, a Killam Research Fellowship, and holds a Canada Research Chair and the Lorne Trottier Chair in Astrophysics and Cosmology. C.-Y.N. is a CRAQ postdoctoral fellow and a Tomlinson postdoctoral fellow.

REFERENCES

- Bernardini, F., Israel, G. L., Stella, L., et al. 2011, *A&A*, 529, A19
- Camilo, F., Ransom, S. M., Halpern, J. P., & Reynolds, J. 2007, *ApJ*, 666, L93
- Dib, R., Kaspi, V. M., & Gavriil, F. P. 2011, *ApJ*, submitted
- Draine, B. T. 2003, *ApJ*, 598, 1026
- Fender, R. P., Muxlow, T. W. B., Garrett, M. A., et al. 2006, *MNRAS*, 367, L6
- Gaensler, B. M., Kouveliotou, C., Gelfand, J. D., et al. 2005, *Nature*, 434, 1104
- Gaensler, B. M., & Slane, P. O. 2006, *ARA&A*, 44, 17
- Gelfand, J. D. 2007, *Ap&SS*, 308, 39
- Gelfand, J. D., & Gaensler, B. M. 2007, *ApJ*, 667, 1111
- Gelfand, J. D., Lyubarsky, Y. E., Eichler, D., et al. 2005, *ApJ*, 634, L89
- Gonzalez, M., & Safi-Harb, S. 2003, *ApJ*, 591, L143

- Granot, J., Ramirez-Ruiz, E., Taylor, G. B., et al. 2006, *ApJ*, 638, 391
- Halpern, J. P., Gotthelf, E. V., Reynolds, J., Ransom, S. M., & Camilo, F. 2008, *ApJ*, 676, 1178
- Harding, A. K., Contopoulos, I., & Kazanas, D. 1999, *ApJ*, 525, L125
- Helfand, D. J., Collins, B. F., & Gotthelf, E. V. 2003, *ApJ*, 582, 783
- Hurley, K., Kouveliotou, C., Cline, T., et al. 1999, *ApJ*, 523, L37
- Israel, G. L., Esposito, P., Rea, N., et al. 2010, *MNRAS*, 408, 1387
- Kaneko, Y., Göğüs, E., Kouveliotou, C., et al. 2010, *ApJ*, 710, 1335
- Kargaltsev, O., & Pavlov, G. G. 2008, in *AIP Conf. Proc. 983, 40 Years of Pulsars: Millisecond Pulsars, Magnetars, and More*, ed. C. Bassa et al. (Melville, NY: AIP), 171
- Kaspi, V. M. 2007, *Ap&SS*, 308, 1
- Kaspi, V. M., Roberts, M. S. E., & Harding, A. K. 2006, in *Compact Stellar X-ray Sources*, ed. W. H. G. Lewin & M. van der Klis (Cambridge: Cambridge Univ. Press)
- Lamb, R. C., & Markert, T. H. 1981, *ApJ*, 244, 94
- Lyutikov, M. 2006, *MNRAS*, 367, 1594
- Mathis, J. S., & Lee, C.-W. 1991, *ApJ*, 376, 490
- Mauche, C. W., & Gorenstein, P. 1986, *ApJ*, 302, 371
- Mereghetti, S. 2008, *A&A Rev.*, 15, 225
- Mereghetti, S., Götz, D., Weidenspointner, G., et al. 2009, *ApJ*, 696, L74
- Murakami, T., Tanaka, Y., Kulkarni, S. R., et al. 1994, *Nature*, 368, 127
- Ng, C.-Y., Kaspi, V. M., Dib, R., et al. 2011, *ApJ*, 729, 131
- Palmer, D. M., Barthelmy, S., Gehrels, N., et al. 2005, *Nature*, 434, 1107
- Predehl, P. & Schmitt, J. H. M. M. 1995, *A&A*, 293, 889
- Rea, N., McLaughlin, M. A., Gaensler, B. M., et al. 2009, *ApJ*, 703, L41
- Scholz, P., & Kaspi, V. M. 2011, *ApJ*, 739, 94
- Strüder, L., Briel, U., Dennerl, K., et al. 2001, *A&A*, 365, L18
- Taylor, G. B., Gelfand, J. D., Gaensler, B. M., et al. 2005, *ApJ*, 634, L93

- Thompson, C., & Blaes, O. 1998, *Phys. Rev. D*, 57, 3219
- Thompson, C., & Duncan, R. C. 1995, *MNRAS*, 275, 255
- Thompson, C., & Duncan, R. C. 1996, *ApJ*, 473, 322
- Thompson, C., Lyutikov, M., & Kulkarni, S. R. 2002, *ApJ*, 574, 332
- Tiengo, A., Vianello, G., Esposito, P., et al. 2010, *ApJ*, 710, 227
- Turner, M. J. L., Abbey, A., Arnaud, M., et al. 2001, *A&A*, 365, L27
- Vink, J., & Bamba, A. 2009, *ApJ*, 707, L148
- Woods, P. M., & Thompson, C. 2006, in *Compact Stellar X-ray Sources*, ed. W. H. G. Lewin & M. van der Klis (Cambridge: Cambridge Univ. Press)

Table 1. Summary of *XMM-Newton* Observations of 1E 1547.0–5408

Date	Obs ID	Exposure (ks)	Count Rate (cnt s ⁻¹) ^a	Mode/Filter ^b
2006 Aug 21	0402910101	38.7	0.074	FF/Medium
2007 Aug 9	0410581901	11.6	0.59	LW/Medium
2009 Feb 3	0560181101	48.9	4.6	FF/Thick
2010 Feb 10	0604880101	35.7	1.9	LW/Medium

^aBackground-subtracted count rate of the point source in the 1–6 keV energy range.

^bThe time resolutions of the operating modes of the EPIC pn camera are: Full Frame (FF): 73.4 ms; Large Window (LW): 47.7 ms.

Table 2. Hardness Ratios for 1E 1547.0–5408 and the Surrounding Extended Emission

Observation	Hardness Ratio ^a		
	Point Source	Region A	Region B
2006	0.306(18)	0.21(6)	0.46(5)
2007	0.482(16)	0.18(5)	0.32(4)
2009	1.014(6)	0.55(4)	0.45(1)
2010	0.814(8)	0.34(4)	0.37(2)

^aThe hardness ratio is defined as $I(3\text{--}6\text{ keV})/I(1\text{--}3\text{ keV})$, where I is the background-subtracted count rate of the point source or extended emission. Numbers in parentheses are 1σ uncertainties.

Table 3. Contribution to Extended Emission Not From Dust-scattering

Region	Count Rate of Extended Emission (cnt s^{-1}) ^a		Fraction Not Attributable to Dust Scattering ^a
	Extrapolated y -intercept ^b	Observed Value in 2006	
A	0.003(1)	0.0085(4)	0.36(12)
B	0.040(3)	0.053(4)	0.75(6)

^aNumbers in parentheses are 1σ uncertainties.

^bExtrapolated y -intercept for the linear fits in Figure 2.

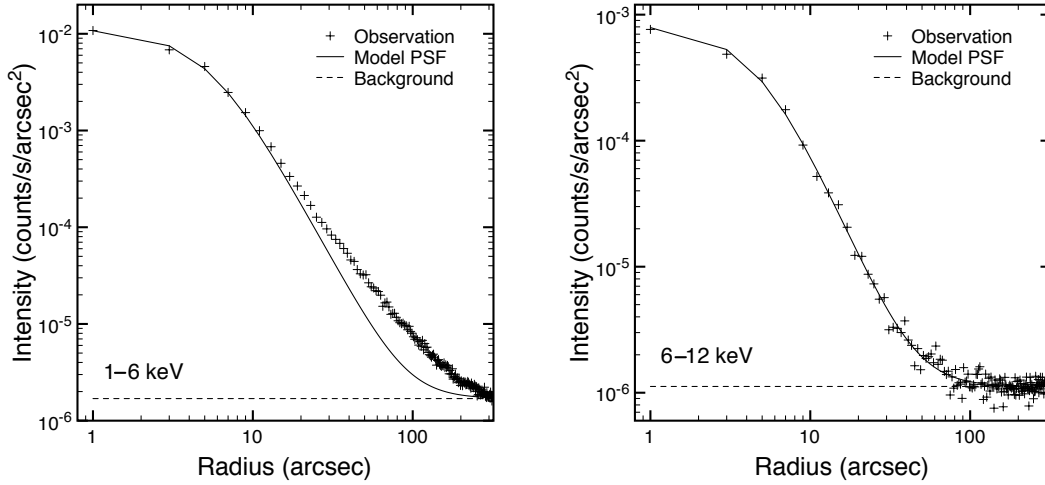


Fig. 1.— Left: 2010 February radial profile of 1E 1547.0–5408 in the 1–6 keV energy band. Right: same but for 6–12 keV.

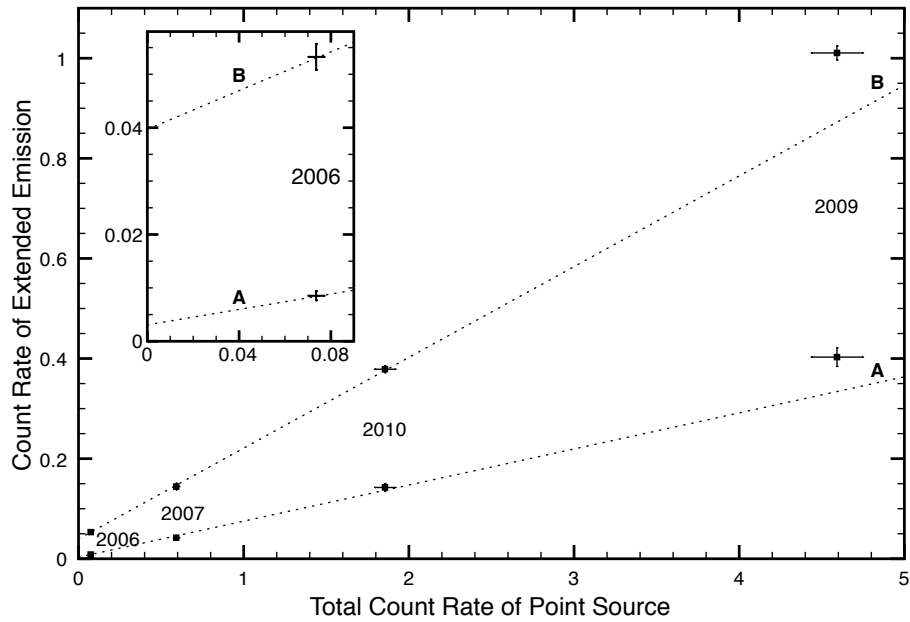


Fig. 2.— 1–6 keV count rate of the extended emission integrated over annular regions with $20'' < r < 40''$ (lower set of points, labeled A) and $40'' < r < 150''$ (upper set of points, labeled B) vs. the total background-subtracted 1–6 keV count rate of the point source for each of the four *XMM-Newton* observations of 1E 1547.0–5408. The dotted lines are fit to the left-most three points. Inset: blow-up of the region near the origin covering the 2006 data points.

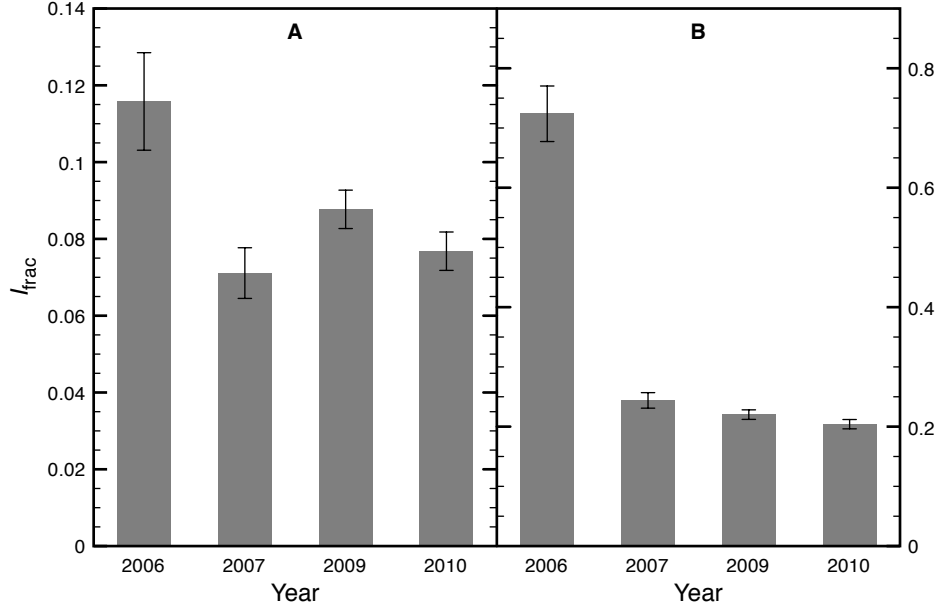


Fig. 3.— Fractional intensity of the extended emission, $I_{\text{frac}} = I_{\text{ext}}/I_{\text{ps}}$, in the 1–6 keV energy band for regions A and B of all four *XMM-Newton* observations of 1E 1547.0–5408.

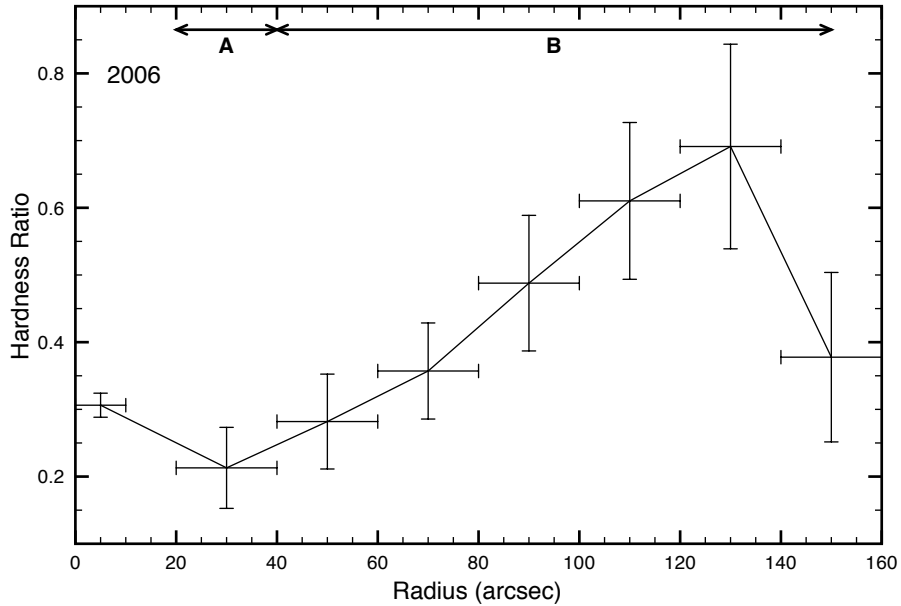


Fig. 4.— Hardness ratio, $\text{HR} \equiv I_{\text{ext}}(3\text{--}6\text{ keV})/I_{\text{ext}}(1\text{--}3\text{ keV})$, for the extended emission of 1E 1547.0–5408 in 2006. The first bin gives the hardness ratio of the point source, whereas all subsequent bins are for the extended emission only. Regions A and B are labeled.